



A simulation study of automotive waste heat recovery using a thermoelectric power generator



Chien-Chou Weng, Mei-Jiau Huang*

Department of Mechanical Engineering, National Taiwan University, Taipei 106, Taiwan

ARTICLE INFO

Article history:

Received 13 December 2012

Received in revised form

8 April 2013

Accepted 8 April 2013

Available online 9 May 2013

Keywords:

Automotive waste heat recovery

Thermoelectric generator

Heat exchanger

ABSTRACT

In this work, an energy-harvesting system which extracts heat from an automotive exhaust pipe and turns the heat into electricity by using thermoelectric power generators (TEGs) was investigated. The influences of the number and the coverage rate on the heat-exchanger of the TEGs were explored via simulations. It was found that implementing more TE couples does not necessarily generate more power in total, and most of all the average power per TE couple decreases rapidly. It is because the wall temperature of the exhaust pipe drops quickly along the streamwise direction and also because the downstream TEGs contend for heat with the upstream TEGs, causing a reduction in the temperature difference between the hot and cold sides of the upstream TEGs. Furthermore, it was also found that for a given total number of TE couples, it is better to retain a portion of the heat exchanger uncovered with TE couples at the downstream side so that the downstream wall of the exhaust pipe uncovered with TE couples becomes even hotter than the upstream wall covered with TE couples. Heat is consequently conducted from the downstream wall to the upstream wall and successively to the attached TEGs; a larger total power can be thus obtained.

© 2013 Elsevier Masson SAS. All rights reserved.

1. Introduction

Because of the global energy crisis and the environmental protection issues, energy recovery techniques have become significantly demanding for a long time. Some examples of energy recovery techniques are water heat recycling, heat recovery ventilation, heat recovery steam generators, and so on [1]. Waste heat recovery by using thermoelectric power generators (TEGs) is another attempt. TEGs can directly convert thermal energy to electrical energy and have the advantages of light weight, no noise, and no mechanical vibration. Owing to these merits, TEGs have found its potential in many applications, such as space applications, thermal energy sensors, textiles, etc. [2–5].

Waste heat originates from various heat sources at different temperatures, such as human bodies, plants, automobiles, and so on [5]. Human body provides low-temperature heat for TEGs. The electrical energy converted from the human-body heat can be applied directly to wearable electronic products such as watches and electronic medical instruments [6,7]. These small-scale applications can be operated by small temperature differences [8]. Waste heats generated from plants and automobiles are at

medium-to-high temperatures and can sustain much larger temperature differences across the TEGs, resulting in large power generation. A 500 kW TEG system for waste heat recovery in a pressurized water reactor power plant was developed by Central Research Institute of Electric Power Industry (CRIEPI) [9]. In addition to the power generation, the reductions in the fuel consumption and in the CO₂ emission resulted by installing TEGs are also noticeable. Chen et al. [10] in use of a Danish district heating system model, estimated the reductions in a system which integrates TEGs into a combined heat and power production (CHP) plant. The results provide useful information for developing energy policies and estimating their environmental impacts.

Waste heat from automotive vehicles is considerable as well. For a typical gasoline-fueled-internal-combustion-engine vehicle, about 40% of the fuel energy is discharged from the exhaust pipe and about 30% is lost into the coolant. Making good use of these waste heats improves the energy efficiency and saves money. Yang [11] indicated that the consumer fuel savings over a three-year period is about \$400 for a 23.5 mpg vehicle, under the assumption of \$2/gallon, 15,000 miles/yr, and a desired 10% fuel-economy improvement (the overall objective raised by the US Department of Energy in 2004). The commonly utilized components in a vehicle for implementing the TEGs are the radiators and the exhaust system. Hsiao et al. [12] established mathematic models and performed experiments; they found a better performance can be

* Corresponding author. Tel.: +886 2 33662696.

E-mail address: mjhuang@ntu.edu.tw (M.-J. Huang).

Nomenclature

c_p	the heat capacity of air	Q_d	the total amount of heat transferred from the downstream side
h_e	the characteristic convection heat transfer coefficient of the heat sink	Q_H	the heat extracted from the hot side of a TEG
\bar{h}	the convection heat transfer coefficient for flat-plate flow	Q_{in}	the input extractable energy
I	the electric current	R_m	the measured electric resistance of a TE couple
K	the thermal conductance of the TEG cuboid	R_{pn}	the electric resistance of a TE couple
k_a	the thermal conductivity of air	Re_{L_c}	the Reynolds number based on the characteristic length L_c
k_m	the effective thermal conductivity of a TEG chip	ΔT	the temperature difference between the hot and cold sides of a TEG
L	the length of the heat exchanger	T_a	the ambient temperature
L_{TEG}	the length of a TEG cuboid	$T_{C,avg}$	the averaged temperature at the cold side of a TEG
L_c	the total length of the simulated system	$T_{H,avg}$	the averaged temperature at the hot side of a TEG
M	the weight of the TEG system	T_{in}	the inlet temperature
\dot{m}	the mass flow rate	ΔT_{leg}	the temperature difference across a TE leg
N	the total number of TE couples in the system	V	the speed of the vehicle
N_x	the number of TE couples along the x -direction in one TEG cuboid	W	the side length of the hexagonal pipe
N_z	the number of the TE couples along the z direction in one TEG cuboid	\dot{W}_{saved}	the saved engine shaft power
\bar{Nu}	the average Nusselt number	α_m	the measured Seebeck coefficient of a TE couple
P	the power generation rate	α_{pn}	the Seebeck coefficient of a TE couple
P_{max}	the maximum power generation rate	$\eta_{alternator}$	the alternator efficiency
Pr	the Prandtl number	η_D	the driveline transmission efficiency
Q_{absorb}	the total amount of heat transferred to the TEGs	$\eta_{exchanger}$	the efficiency of the exchanger
Q_C	the heat dissipated at the cold side of a TEG	η_{PCU}	the Power Conditioning Unit (PCU) efficiency
		$\eta_{recovery}$	the recovery efficiency
		η_{TEG}	the efficiency of the TEG
		μ_r	the rolling resistance coefficient

obtained by attaching TEGs to the exhaust system than to the radiators. Directly attaching TEGs to the original equipments in the exhaust system, such as the catalytic converter [13], the muffler, the exhaust pipe, and so forth, is one way to go. Alternatively one can construct a heat exchanger to extract heat from the exhaust pipe to the integrated TEGs.

Depending on the kind of the cooling system, the TE materials, the system size, and the operating conditions, the power generation rate differs in the literature. The Hi-Z Technology, Inc. [14] attached TEGs on the outer surface of an octagonal cast-steel heat exchanger with a hollow displacement body in the center and used eight aluminum water-cooled-heat-sink assemblies. By installing swirl fins on the displacement body and using seventy-two HZ-13 Bi_2Te_3 modules, they obtained 1 kW from a Cummins NTC 350 Diesel engine operated at 300 HP and 1700 RPM. In 2001, in order to solve mechanical problems during the road test, HZ-14 modules were built. A maximum electric power of 900 W was obtained from a Cummins 335 Diesel engine operated at 290 HP and 2100 RPM [15]. Crane and Lagrandeur [16] built a single-layer high-temperature segmented TEG with the most suitable thermoelectric materials for various operating temperature ranges. A power as large as 125 W was obtained by extracting heat from a hot air at 600 °C and at a flow rate of 45 cfm and using a cooling water at 25 °C and at a flow rate of 10 lpm. Karri et al. [17] simulated a TEG-integrated sports utility vehicle which includes sixteen HZQW (quantum-well materials, Si/SiGe and $\text{B}_4/\text{B}_9\text{C}$) TEG chips. The water coolant system in the vehicle was also used to cool the TEG system. About 450 W was generated at a vehicle speed of 112.7 km/h and about 1.5% fuel savings was obtained after the consideration of the coolant-pumping power loss, blow-down power loss, and the power loss to transport the weight of the TEG system; the fuel saving of the car using Bi_2Te_3 TEGs is negative nonetheless. Hsu et al. [18] proposed a heat exchanger mounted with eight Bi_2Te_3 –TEG chips and employed eight air-cooled-heat-sink assemblies. A maximum power of 44 W was obtained. In 2012, they enlarged the heat

exchanger with a similar interior structure and added a sloping block in the inlet [19]. A maximum power of 12 W was obtained instead when twenty-four TEG chips and twenty-four air-cooled-heat-sink assemblies were implemented. Their experimental results surprisingly suggest that a small-size heat exchanger with less TEGs can generate more power.

Most of the studies mentioned above focused on the design of the heat exchangers and the development of the TEG modules. However, according to Hsu's study, the size of the heat exchanger and the number of the TE couples implemented are two other factors that may strongly affect the power generation efficiency. Therefore, the influences of these two factors are of interest in the present work. The investigation was executed by performing full three dimensional simulations in use of the commercial software ANSYS-Fluent. A heat exchanger similar to that employed by the Hi-Z Technology, Inc. [14] was employed. As its total length and the coverage rate with the TE couples were varied, the power generation rate was computed. The optimization of these two parameters is aimed at.

The rest of this paper introduces the simulation model in Section 2, presents the simulation results and discussions in Section 3, and finally gives the conclusion in Section 4.

2. Numerical experiment

2.1. Simulation model

The energy harvesting system consists of a heat exchanger and TEGs as shown in Fig. 1. The heat exchanger, composed of a hexagonal pipe, radial fins, and a hollow center body, is connected to the exhaust pipe of diameter 62 mm on both sides. The hexagonal pipe has an inscribed circle of diameter 140 mm and a length of L . It is connected to the exhaust pipe via a divergent/convergent part. The hollow center body, including a circular pipe of diameter 100 mm and length L as well as two bullet-shape heads of length

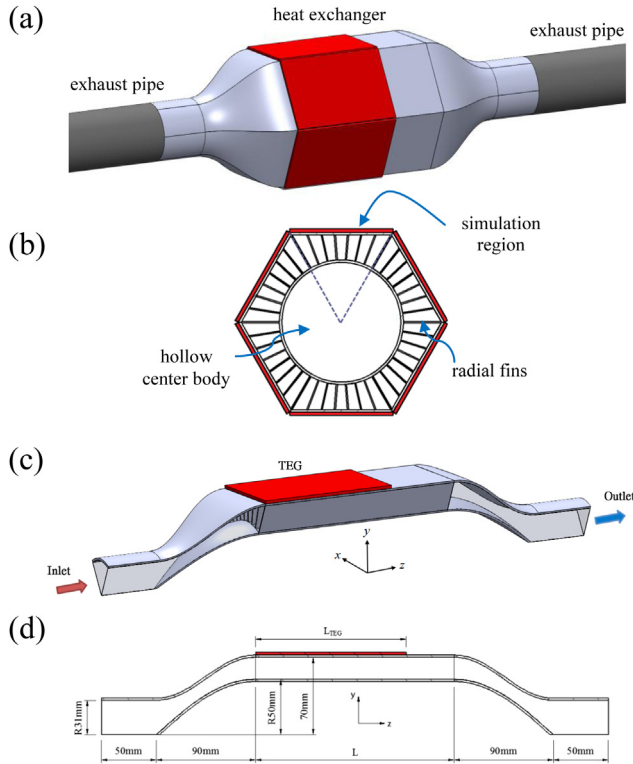


Fig. 1. The energy harvesting system: (a) a three dimensional chart, (b) an x - y cross-sectional view, (c) the simulation domain (one-sixth of the system), (d) the dimensions on the cross section of $x = 0$.

90 mm, is supported by the radial fins of thickness 1 mm, which are connected to the inner surface of the hexagonal pipe on the other end. All of the solid components are made of aluminum. Finally, TEGs of length L_{TEG} (colored by red in Fig. 1) are attached to the outer surfaces of the hexagonal pipe, starting from the most upstream edge.

2.2. Simulation method

Because of the symmetry of the energy-harvesting system, only one-sixth of the system needs simulating. An unstructured mesh system, which is composed of about 3.5×10^6 cells and about 1.8×10^6 nodes, was carefully built. The SIMPLE algorithm and second-order upwind scheme were used to solve the steady-state heat transfer problem. The realizable k - ϵ turbulence model was adopted, in which the dissipation rate equation is derived from the dynamic equation of the mean-square vorticity fluctuation at large turbulent Reynolds number [20]. The convergence criteria adopted herein are a scaled residual under 10^{-3} for the momentum balance, 10^{-6} for the energy balance, and a relative error under 0.1% for the total energy conservation of the system.

The boundary conditions are illustrated in Fig. 2. The no-slip boundary conditions are imposed at all the solid walls. The inlet

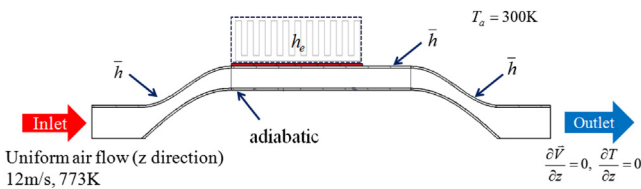


Fig. 2. The boundary conditions employed in this study.

boundary condition, referring to Hsu et al. [18], is a uniform flow of velocity 12 m/s and temperature $T_{in} = 773$ K. Imposed at the outlet boundary are zero gradients for velocity and temperature. The inner surface of the center body is adiabatic. The heat sink attached to the cold side of the TEG was not simulated but modeled by a characteristic convection heat transfer coefficient h_e . In this study, attempted are two values, 600 W/m² K and 1800 W/m² K, which characterize the S2090-40W heat sink produced by Alpha Company Ltd. operated at an air velocity of 1 m/s and 5 m/s respectively [21]. The rest of the outer surface of the heat exchanger on the other hand has a convection heat transfer coefficient of $\bar{h} = 60$ W/m² K. This value is obtained based on the following empirical equation [22]:

$$\overline{Nu} = \frac{\bar{h}L_c}{k_a} = Pr^{1/3} (0.037 Re_{L_c}^{0.8} - 871) \quad (1)$$

for flat-plate flows with $L_c = 460$ mm (the total length of the energy harvesting system when $L = 180$ mm; see Fig. 1d), an air velocity of 30 m/s (about the car speed on the freeway), and air properties evaluated at the ambient temperature $T_a = 300$ K, where appear the air thermal conductivity k_a , the Prandtl number Pr , and the Reynolds number Re_{L_c} . As the heat exchanger length L varies from 50 mm to 240 mm, Eq. (1) gives a value of \bar{h} ranging from 53 W/m² K to 65 W/m² K. The variation is small. For convenience, we adopt a fixed value of $\bar{h} = 60$ W/m² K in all the simulations. Finally, the exhaust gas was modeled as air whose properties vary with temperature, and the TEG was modeled as a cuboid of thickness 2.8 mm with an effective thermal conductivity of $k_m = 3.26$ W/m K [18,19].

2.3. Power calculation

Once the simulated system has reached steady, the temperature difference between the hot and cold sides of the TEG cuboid ($T_{H,avg}$ and $T_{C,avg}$) was extracted to compute the power generation rate. The generated power of a TEG is generally expressed as

$$P = N\alpha_{pn}I\Delta T_{leg} - I^2NR_{pn}, \quad (2)$$

where ΔT_{leg} is the temperature difference across the TE leg, N is the number of TE couples employed, I is the electric current, α_{pn} is the Seebeck coefficient, and R_{pn} is the internal electric resistance of one TE couple. However, instead of the temperature difference across the TE leg, it is usually the temperature difference between the two ceramic plates of a TEG chip (ΔT) that is measured. Besides, the copper plate, the contact thermal as well as electric resistances, and the heat loss due to convection and radiation heat transfers all may cause a loss in the output power. We thus, in evaluating the power generation rate, adopt the measured Seebeck coefficient α_m and the measured electric resistance R_m (see Table 1) of the TEG chips employed by Hsu et al. [23], each of which is composed of 199 Bi₂Te₃–TE couples.

On the other hand, because the cross section of a single TE couple is about 3.77 mm × 3.77 mm, the total number of TE couples implemented are $N = 6N_z \times N_x$, where $N_z = L_{TEG}/3.77$ mm and $N_x = W/3.77$ mm with $W = 48\sqrt{3}$ mm being the side length of the

Table 1
The thermoelectric properties of the employed TEG chips [23].

α_m	295 μ V/K
R_m	6.48 m Ω
k_m	3.26 W/m K

Table 2

The simulation results when $L = L_{\text{TEG}} = 180$ and $h_e = 1800 \text{ W/m}^2 \text{ K}$.

$K\Delta T_{\text{avg}}$	4836 W
$T_{\text{H,avg}}$	375.9 K
$T_{\text{C,avg}}$	329.5 K
ΔT_{avg}	46.16 K

hexagonal pipe. The maximum power generation rate, which can be obtained by selecting an external load resistance equal to the total internal electric resistance (NR_m), and the corresponding electric current therefore become

$$P_{\text{max}} = 3.36 \times 10^{-6} \cdot N\Delta T_{\text{avg}}^2 \text{ (W)} \quad (3)$$

and

$$I = \alpha_m \Delta T_{\text{avg}} / (2R_m) \quad (4)$$

with ΔT_{avg} being the averaged temperature difference between the hot and cold sides of the TEG cuboid.

There is one more issue that needs addressing before we end this section. In the present simulations, we did not consider the Joule's heat and Peltier heat; that is, an open-circuit system was simulated. The so-obtained temperature difference ΔT_{avg} was then employed to evaluate the power generation rate by using Eq. (3). It is known however that ΔT_{avg} actually varies with the external load resistance or the generated electric current due to the Peltier and Joule heat. To estimate the induced error, we take the system having $L = L_{\text{TEG}} = 180$ mm and $h_e = 1800 \text{ W/m}^2 \text{ K}$ for example. The temperatures at the hot and cold sides of the TEG and the heat conducted to the TEG obtained from the open-circuit simulation are listed in Table 2. We now consider an imaged close-circuit system within which the temperatures at the hot and cold sides of the TEG are as the same as those in the open-circuit system. The heat extracted from the hot side (Q_H) and the heat dissipated at the cold side (Q_C) of a TEG in the close-circuit system, namely,

$$Q_H = N\alpha_m I T_{\text{H,avg}} + K\Delta T_{\text{avg}} - \frac{1}{2}I^2 NR_m, \quad (5a)$$

$$Q_C = N\alpha_m I T_{\text{C,avg}} + K\Delta T_{\text{avg}} + \frac{1}{2}I^2 NR_m \quad (5b)$$

are found to be $Q_H = 5537 \text{ W}$ and $Q_C = 5492 \text{ W}$; the values of the Peltier and Joule heat at both sides are thus 701 W and 656 W respectively, which are about 14% of the conduction heat $K\Delta T_{\text{avg}}$ (K is the thermal conductance of the TEG cuboid).

3. Result and discussion

In the following two subsections, we investigate the influence of the heat-exchanger length (L) and its coverage rate with the TE

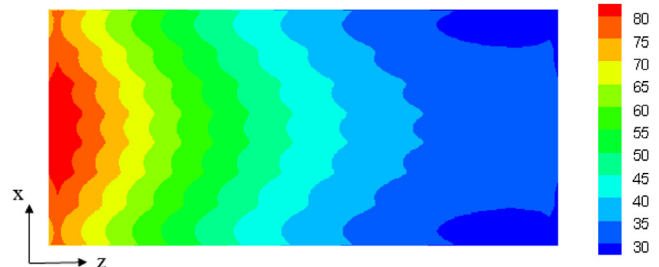


Fig. 4. The distribution of the temperature difference between the hot and cold sides of the TEG cuboid in a system in which $L = L_{\text{TEG}} = 180$ mm and $h_e = 1800 \text{ W/m}^2 \text{ K}$.

couples on the generated power separately. In the former, the performances of the heat exchangers of various lengths, completely covered by TE couples, were compared. In the latter, we fixed the total number of the TE couples and changed the coverage rate by varying the length of the heat exchanger. A comparison between the completely and partially covered situations was made in Section 3.3. The waste-heat recovery efficiency was discussed in Section 3.4.

3.1. Effect of the length of the heat exchanger completely covered with TE couples

In this subsection, we make the outer surfaces of the heat exchanger completely covered by the TE couples; that is $L = L_{\text{TEG}}$. Intuitively one expects the longer the heat exchanger length, the more TE couples are installed, and consequently the more power is generated. Five different lengths, 50 mm, 80 mm, 120 mm, 180 mm, and 240 mm, were attempted. Fig. 3 shows the x - y and y - z cross-sectional temperature distributions of the system having $L = L_{\text{TEG}} = 180$ mm and $h_e = 1800 \text{ W/m}^2 \text{ K}$. Fig. 4 shows the distribution of the temperature difference between the hot and cold sides of the TEG cuboid. As seen, because of the cooling effect (by h_e), the temperature of the exhaust air decreases rapidly along the streamwise direction; so is the temperature difference between the hot and cold sides of the TEG cuboid. The temperature difference variation in the x direction is much smaller (Fig. 4), so we averaged the temperature difference along the x direction and observed its variation in the z direction as shown in Fig. 5. It is observed that the temperature difference decreases with the downstream distance due to the drop in the fluid temperature. Furthermore, the temperature difference at a fixed downstream distance decreases with increasing heat-exchanger length. This is because the strong heat sinks mounted at the downstream TEGs attract heat to be conducted from the upstream side to the downstream side via the solid components in the system. Consequently the longer the heat-exchanger length, the less heat is conducted to the upstream TE couples and the smaller the upstream temperature difference becomes. Finally, without surprise the stronger the heat sink, the larger the temperature difference is.

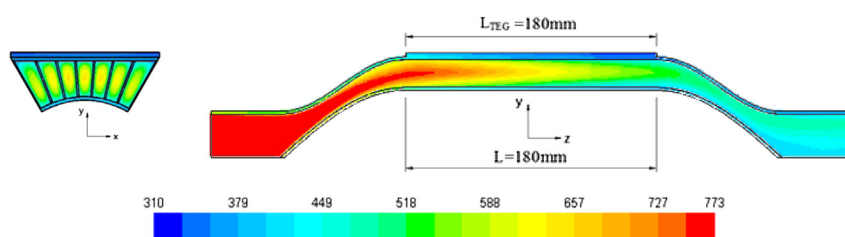


Fig. 3. The x - y and y - z cross-sectional temperature distributions in a system in which $L = L_{\text{TEG}} = 180$ mm and $h_e = 1800 \text{ W/m}^2 \text{ K}$.

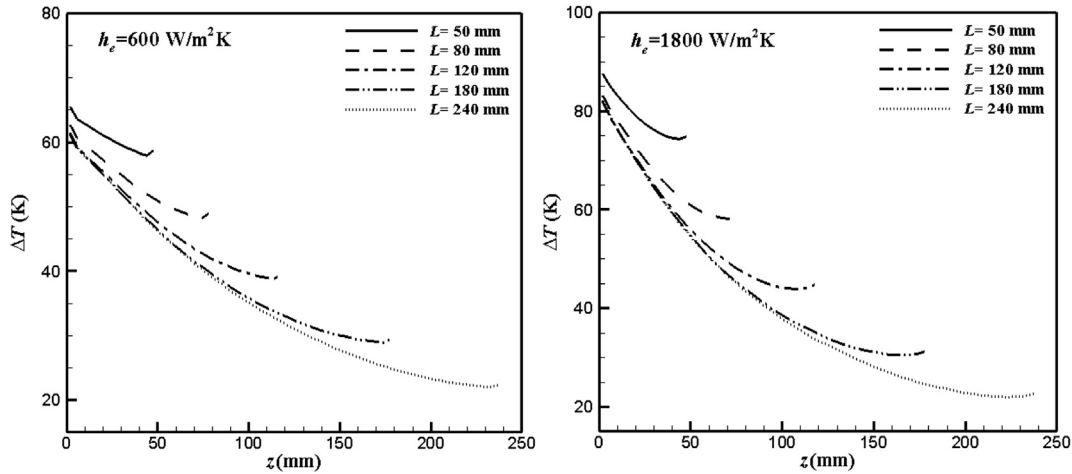


Fig. 5. The distributions of the temperature difference between the hot and cold sides of the TEG cuboid along the z -direction when the heat exchanger is completely covered with TE couples.

We now calculate the total power generation rate and the average power generation rate per TE couple according to Eq. (3). The results are shown in Fig. 6. As expected, the total power increases with the increasing heat-exchanger length or the increasing number of TE couples but gets saturated quickly. However, the average power per TE couple has an opposite variation trend. This is because the total power generation is proportional to the total number of TE couples but to the square of the temperature difference; increasing the heat-exchanger length increases the number of TE couples but decreases the temperature difference as discussed above.

3.2. Effect of the length of the heat exchanger partially covered with TE couples

We now try to cover the outer surface of the heat exchanger with TE couples partially. We fixed the length of the TEG cuboid, L_{TEG} , at 50 mm and varied the length of the heat exchanger. The x -averaged temperature differences between the hot and cold sides of the TEG cuboid are shown in Fig. 7. It shows that the temperature difference increases with the heat exchanger length and it decreases first but

increases later near the downstream edge of the TEG cuboid along the downstream distance. A further examination on the wall temperature of the heat exchanger as shown in Fig. 8 finds the downstream wall without TE couples mounted (black curves) has a higher temperature than the upstream wall with TE couples mounted (red curves) due to a smaller convection heat transfer coefficient ($h = 60 \text{ W/m}^2 \text{ K}$) over there. Heat is therefore transferred to the endmost TEGs not only from the hot fluid but also from the hotter downstream wall; a larger temperature difference is consequently resulted. We distinguished and listed the amounts of heat transferred to the TEGs in Table 3, where Q_{absorb} denotes the total amount of heat transferred to the TEGs and Q_d is the amount transferred from the downstream side. As seen, Q_d can reach as much as 13% of Q_{absorb} when $h_e = 600 \text{ W/m}^2 \text{ K}$ and 17% when $h_e = 1800 \text{ W/m}^2 \text{ K}$. Besides, Q_d increases with the heat-exchanger length but quickly gets saturated. This explains the rapid saturation observed in the temperature difference and the total power generation rate (Fig. 9). From the economic consideration, an incomplete coverage is superior to a complete coverage and a heat exchanger slightly longer than twice the length of the TEG cuboid is sufficient; the latter is suggested from the dashed line indicated in Fig. 9.

3.3. Comparison between completely and partially covered situations

The comparison of these two situations is shown in Fig. 10. The length of the heat exchanger (L) is fixed at 180 mm and the length of the TEG cuboid (L_{TEG}) is varied in the partially covered situation. Fig. 10 shows with the same number of TE couples, the partial covered case always performs better than the completely covered one; the difference increases with the increasing strength of the heat sink and decreases with the increasing length of the TEG cuboid, or with the relatively decreasing length of the heat exchanger. The total power in the partially covered case with $L_{\text{TEG}} = 80 \text{ mm}$ is larger than that in the completely covered case with $L_{\text{TEG}} = 180 \text{ mm}$ when $h_e = 1800 \text{ W/m}^2 \text{ K}$. It implies a larger power can be generated with less TE couples by simply making the heat exchanger longer than the TEG cuboid. Fig. 11 shows again that the temperature difference between the hot and cold sides of the TEG cuboid at a fixed downstream distance is smaller and the up-trend near the downstream edge of the TEG cuboid becomes less obvious when the TEG cuboid is longer or the uncovered part of the heat exchanger is shorter. All these observations are consistent with those found in the last subsections and are strongly correlated

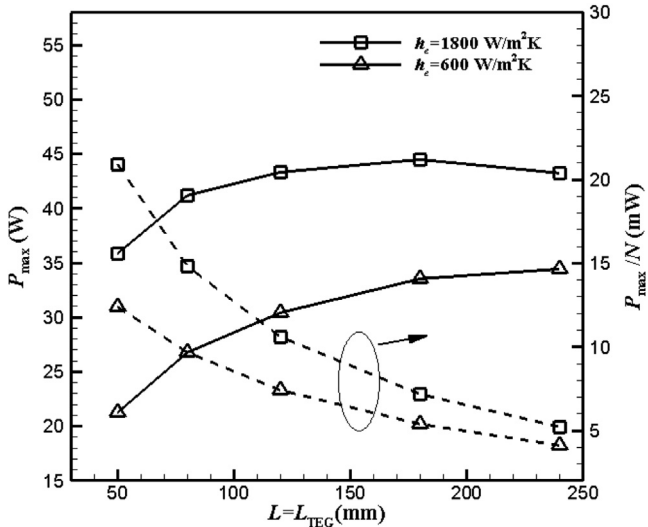


Fig. 6. The total power (solid lines) and the average power per TE couple (dash lines) against the heat-exchanger length L when the heat exchanger is completely covered with TE couples.

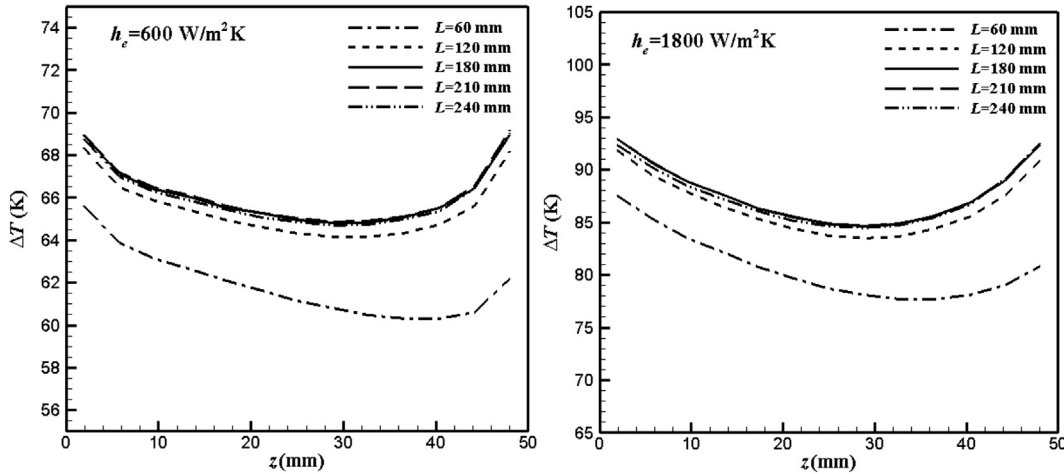


Fig. 7. The distributions of the temperature difference between the hot and cold sides of the TEG cuboid along the z direction when the heat exchanger is partially covered with TE couples.

to the fact that the strong heat sinks make cooler the wall where they are attached so as to loot heat from the neighboring hotter wall. Consequently, adding more TE couples at the downstream side generates an additional power but also reduces the upstream temperature difference and consequently the power generation of the upstream TE couples. The additional power by the downstream TE couples is thus offset by the reduced power of the upstream TE couples. The total power gets saturated or even turns decreasing eventually as observed from Figs. 6 and 10.

3.4. Waste-heat recovery efficiency

Among all the energy harvesting systems performed herein, the maximum total power (P_{\max}) is about 48 W and the total heat transferred to the TEG cuboids is about 3.3 kW when the heat exchanger of length 180 mm is partially covered with TEGs of length 80 mm and the heat sink of strength $h_e = 1800 \text{ W/m}^2 \text{ K}$ is employed. The input extractable energy may be expressed as

$$Q_{\text{in}} = \dot{m}c_p(T_{\text{in}} - T_a), \quad (6)$$

where \dot{m} is the mass flow rate and c_p is the heat capacity of air at $(T_{\text{in}} + T_a)/2$. In all of our simulations, Q_{in} is 8.2 kW. The efficiency of the heat exchanger ($\eta_{\text{exchanger}} = Q_{\text{absorb}}/Q_{\text{in}}$) is about 40%, the conversion

Table 3

The total amount of the heat transferred to the TEG cuboid (Q_{absorb}) and the part transferred from the downstream side (Q_d).

L (mm)	60	120	150	180	210	240
$h_e = 600 \text{ W/m}^2 \text{ K}$						
Q_d (W)	95	226	243	250	253	250
Q_{absorb} (W)	1816	1921	1933	1941	1943	1938
Q_d/Q_{absorb}	5%	12%	13%	13%	13%	13%
$h_e = 1800 \text{ W/m}^2 \text{ K}$						
Q_d (W)	223	404	426	437	439	445
Q_{absorb} (W)	2354	2524	2544	2559	2560	2552
Q_d/Q_{absorb}	10%	16%	17%	17%	17%	17%

efficiency of the TEG ($\eta_{\text{TEG}} = P_{\max}/Q_{\text{absorb}}$) is about 1.5%, and the recovery efficiency ($\eta_{\text{recovery}} = P_{\max}/Q_{\text{in}}$) is about 0.6%. These efficiencies are relatively low compared to the existing ones in the literature, mainly because the whole system is not optimized yet. For instance, a replacement of the air cooling system by a water cooling system or a use of a highly efficient heat exchanger (such as counter-current heat exchangers) can improve the performance significantly. Nonetheless, the present investigation highlights the existence of an optimum coverage rate of TE couples on the heat exchanger.

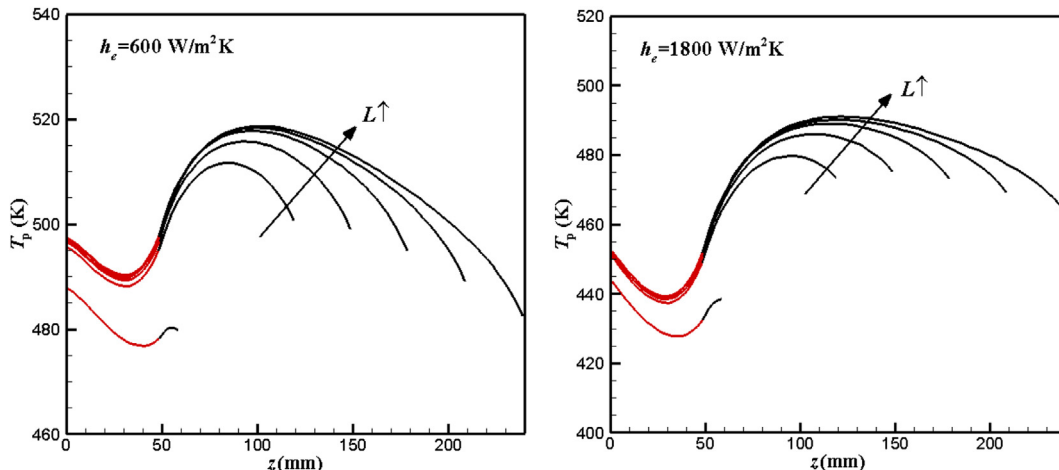


Fig. 8. The wall temperature distributions of the heat exchanger along the z direction. The section attached with TE couples is colored by red. (For interpretation of the references to color in this figure legend, the reader is referred to the web version of this article.)

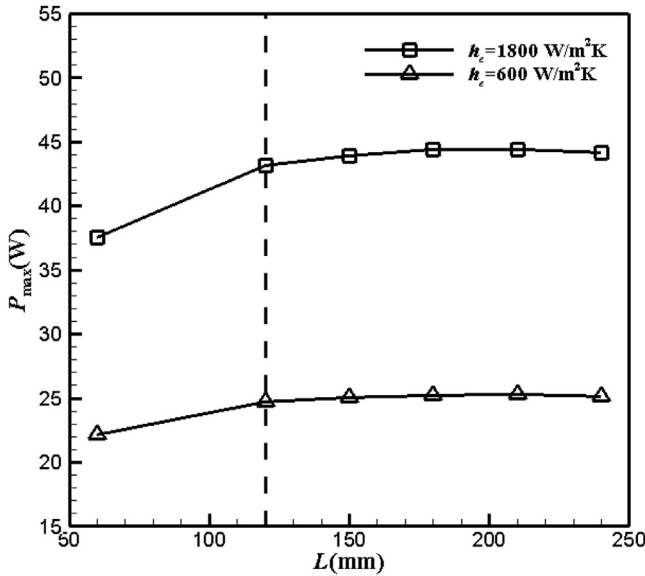


Fig. 9. The total power generation rate against the length of the heat exchanger when the length of the TEG cuboid (L_{TEG}) is fixed at 50 mm.

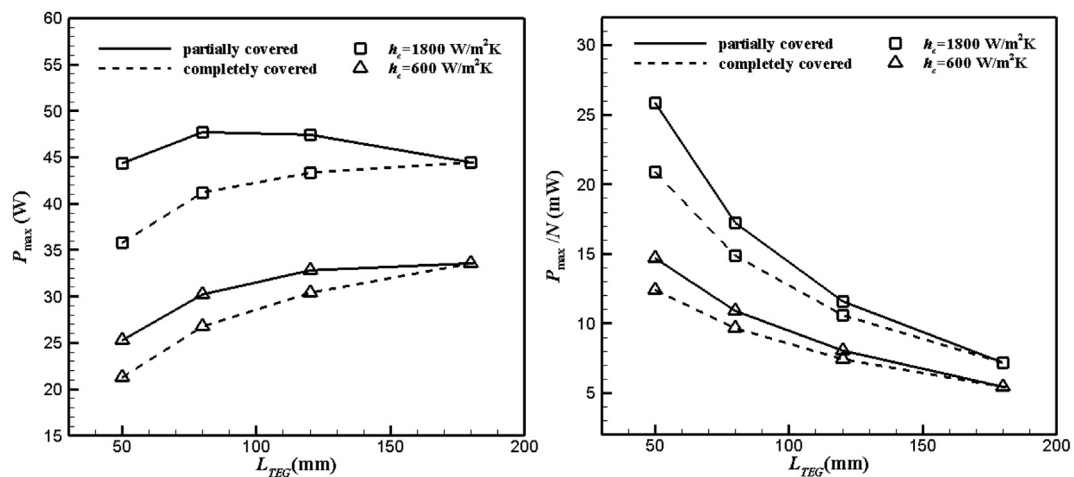


Fig. 10. The total power and the average power per TE couple against the length of the TEG cuboid, L_{TEG} ; $L = 180$ mm is fixed in the partially covered situation.

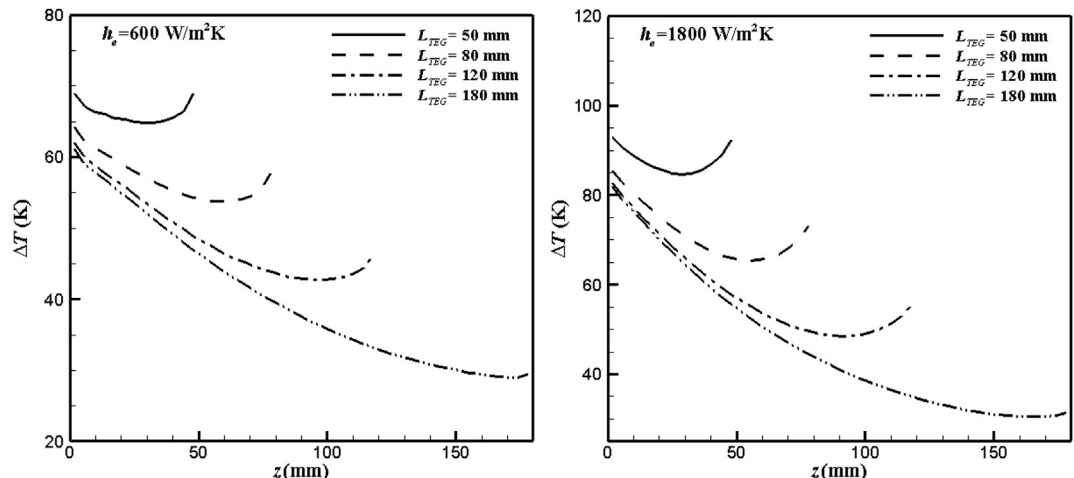


Fig. 11. The distributions of the temperature difference between the hot and cold sides of the TEG cuboid along the z direction when the heat exchanger length (L) is fixed at 180 mm.

At last, we make some discussions about the saving of the engine shaft power by installing such a TEG energy harvesting system. The installation of the TEG system generates additional electric power, but also causes some parasitic power loss, such as blow-down power loss due to the backpressure increase of the engine and the power loss due to the increased weight by the TEG system. In the maximum-power case discussed above, the induced pressure drop is about 25 Pa, much smaller than the pressure drop across the muffler which is about 30 kPa [24]. Karri et al. [17] also indicated the dominant loss arises from the increased weight of the TEG system. According to Karri et al. [17], the saved engine shaft power may be evaluated by the following formula:

$$\dot{W}_{\text{saved}} = \frac{\eta_{\text{PCU}} P_{\text{max}}}{\eta_{\text{alternator}}} - \frac{\mu_r M V}{\eta_D}, \quad (7)$$

where appear the rolling resistance coefficient μ_r , the weight of the TEG system M , the speed of the vehicle V , the driveline transmission efficiency η_D , the Power Conditioning Unit (PCU) efficiency η_{PCU} , and the alternator efficiency $\eta_{\text{alternator}}$. By using their parameters as rearranged in Table 4 and substituting a vehicle velocity of 30 m/s and a weight of 4.5 kgw (the weight of the maximum-power system including the aluminum heat exchanger and the S2090-40W heat sinks [21]) into the formula, the saved engine shaft power is about 67 W.

Table 4

The values of the parameters employed for evaluating the saved engine shaft power.

μ_r [17]	0.012
η_D [17]	0.9
η_{PCU} [17]	0.88
$\eta_{alternator}$ [17]	0.5

4. Conclusion

In this work, a heat exchanger attached with TEGs for recovering waste heat from an automotive exhaust pipe was investigated by using the commercial software ANSYS-Fluent. It was found the heat sinks attached to the downstream TEGs possibly cause the downstream wall cooler which thus loots heat from the upstream hotter wall, resulting in a degradation of the performance of the upstream TEGs. Consequently implementing more TE couples may not necessarily be worthwhile economically. Leaving some downstream part of the heat exchanger uncovered with the TE couples on the other hand results in a hotter downstream wall, more heat transferred to the upstream TE couples, and consequently a larger power generation rate. A saturation of the power generation occurs nonetheless when the TEG-uncovered part of the heat exchanger is sufficiently long. This investigation reveals a new parameter to optimize the energy harvesting system—the number of the employed TEG chips, once the heat exchanger, the cooling system, and the thermoelectric material have been carefully determined. For the heat exchanger investigated herein, the optimum length of the TEG cuboid is 80 mm for a heat exchanger of length 180 mm, and the optimum length of the heat exchanger is 120 mm for a TEG cuboid of length 50 mm, when the convection heat transfer coefficient associated with the heat sink is $1800 \text{ W/m}^2 \text{ K}$.

Acknowledgment

This work was supported by the National Science Council of Taiwan (Grant No. NSC 100-2221-E-002-143-MY3).

References

- [1] Y. Demirel, Energy: Production, Conversion, Storage, Conservation, and Coupling, Springer, 2012.
- [2] S.B. Riffat, X. Ma, Thermoelectrics: a review of present and potential applications, *Appl. Therm. Eng.* 23 (2003) 913–935.
- [3] T. Xu, H. Huang, W. Luan, Y. Qi, S.T. Tu, Thermoelectric carbon monoxide sensor using Co–Ce catalyst, *Sens. Actuators B* 133 (2008) 70–77.
- [4] M. Plissonnier, C. Salvi, T. Lanier, D. Coulaux, Thermoelectric Structure and Use of the Thermoelectric Structure to Form a Textile Structure, US Patent 0029146A1, 2008.
- [5] K.M. Saqr, M.N. Musa, Critical review of thermoelectrics in modern power generation applications, *Therm. Sci.* 13 (2009) 165–174.
- [6] V. Leonov, R.J.M. Vullers, Thermoelectric generators on living beings, in: Proc. 5th European Conf. on Thermoelectrics, Odessa, Ukraine, 2007, pp. 47–52.
- [7] V. Leonov, R.J.M. Vullers, Wearable thermoelectric generators for body-powered devices, *J. Electron. Mater.* 38 (2009) 1491–1498.
- [8] N.S. Hudak, G.G. Amatucci, Small-scale energy harvesting through thermoelectric, vibration, and radiofrequency power conversion, *J. Appl. Phys.* 103 (2008) 101301.
- [9] M. Kambe, A Concept of 500 kW Thermoelectric Power Conversion System to Make Use of Waste Heat of PWR Power Plant. Annual Research Report, Central Research Institute of Electric Power Industry, Japan, 2004.
- [10] M. Chen, H. Lund, L.A. Rosendahl, T.J. Condra, Energy efficiency analysis and impact evaluation of the application of thermoelectric power cycle to today's CHP systems, *Appl. Energy* 87 (2010) 1231–1238.
- [11] J. Yang, Potential applications of thermoelectric waste heat recovery in the automotive industry, in: Proc. 24th Int. Conf. on Thermoelectrics, Clemson, South Carolina, USA, 2005, pp. 170–174.
- [12] Y.Y. Hsiao, W.C. Chang, S.L. Chen, A mathematic model of thermoelectric module with applications on waste heat recovery from automobile engine, *Energy* 35 (Dec. 2010) 1447–1454.
- [13] S. Kwak, C.A. Willner, G. Konstantakopoulos, Integrated Thermoelectric Power Generator and Catalytic Converter, US Patent 0223919A1, 2003.
- [14] J.C. Bass, N.B. Elsner, F.A. Leavitt, Performance of the 1 kW Thermoelectric Generator for Diesel Engines, Hi-Z Technology, Inc., 1994.
- [15] A.S. Kushch, J.C. Bass, S. Ghamaty, N.B. Elsner, Thermoelectric development at Hi-Z technology, in: Proc. 20th Int. Conf. on Thermoelectrics, Beijing, China, 2001, pp. 422–430.
- [16] D.T. Crane, J.W. Lagrandeur, Progress report on BSST-led US department of energy automotive waste heat recovery program, *J. Electron. Mater.* 39 (2010) 2142–2148.
- [17] M.A. Karri, E.F. Thacher, B.T. Helenbrook, Exhaust energy conversion by thermoelectric generator: two case studies, *Energy Convers. Manage.* 52 (2011) 1596–1611.
- [18] C.T. Hsu, D.J. Yao, K.J. Ye, B. Yu, Renewable energy of waste heat recovery system for automobiles, *J. Renew. Sustain. Energy* 2 (2010) 013105.
- [19] C.T. Hsu, G.Y. Huang, H.S. Chu, B. Yu, D.J. Yao, Experiments and simulations on low-temperature waste heat harvesting system by thermoelectric power generators, *Appl. Energy* 88 (2011) 1291–1297.
- [20] T.H. Shih, W.W. Liou, A. Shabbir, Z. Yang, J. Zhu, A new $k-\varepsilon$ eddy viscosity model for high Reynolds number turbulent flow, *Comput. Fluids* 24 (1995) 227–238.
- [21] http://www.micforg.co.jp/en/c_s2090e.html.
- [22] Y.A. Cengel, Heat and Mass Transfer: a Practical Approach, third ed., McGraw-Hill, New York, 2006.
- [23] C.T. Hsu, G.Y. Huang, H.S. Chu, B. Yu, D.J. Yao, An effective Seebeck coefficient obtained by experimental results of a thermoelectric generator module, *Appl. Energy* 88 (2011) 5173–5179.
- [24] http://www.thrashercharged.com/tech_htm/exhaust.shtml.